Supporting Information

Conductive Metal-Covalent Organic Frameworks as Novel Catalytic Platform for Reduction of Nitrate to Ammonia

Hao Huang, Kaiying Wang*

H. Huang and Prof. Kaiying Wang
Department of Microsystems
University of South-Eastern Norway
Borre 3184, Norway
E-mail: Kaiying.Wang@usn.no

Experimental Section

physical characterization

Powder X-ray diffraction (XRD) patterns of various c-MCOFs nanosheets were measured by Bruker D8 Advance with Cu-Kαradiation (40 KV, 40 mA, λ = 0.15418 nm). Bruker ASCEND NMR Spectrometer (400 MHz) was employed for their nuclear magnetic resonance (NMR) spectra. HITACHI SU8020 field-emission electron microscope was used to record the scanning electron microscopy (SEM) images for investigating the morphology and the energy dispersive X-Ray spectroscopy (EDS) mapping for analyzing the element composition. Meanwhile, the transmission electron microscopy (TEM) images were obtained by TECNAI F20 transmission electron microscope. X-ray photoelectron spectroscopy (XPS) technology was utilized to investigate the chemical states of various c-MCOFs samples by PHI-5000 X-ray photoelectron spectrometer. PerkinElmer Lambda 650 spectrophotometer was used for measure the concentrations of electrochemical products in electrolyte by an ultraviolet-visible (UV-vis) chromogenic method.

electrochemical measurements

The nitrate reduction to Ammonia (NRA) properties of various c-MCOFs samples were investigated by electrochemical workstation (CHI 760E; Shanghai) with standard three-electrode system. Carbon papers, coated by c-MCOFs samples, were used as working electrode; graphite rod and saturated calomel electrode (SCE) were worked as the counter electrode and reference electrode, respectively. In this work, a typical H-type electrolytic cell was utilized; in particular, Nafion 117 membrane was employed to separate the cathode and anode in this electrolytic cell. Before electrochemical test, the Nafion 117 membrane need a pre-treatment. The Nafion 117 membrane was boiled in 3% H_2O_2 for 30 min to remove organic impurities. The membrane surface of Nafion 117 was repeatedly cleaned with deionized water, and then boiled in 0.5 M H_2SO_4 for another 1 h. The membrane was stored in deionized water for later use. After each electrochemical reaction, the membrane was placed in deionized water for 30 seconds each time for 3 times to remove residual impurities and contaminants on the surface to avoid affecting the results of the next experiment. All SCE potentials were transferred to RHE via the Nernst equation:

$$E_{RHE} = E_{SCE} + 0.244 + 0.059pH \tag{1}$$

In this work, 70 mL of 0.5 M Na_2SO_4 solution with 0.1 M $NaNO_3$ is used as electrolyte for the cathode and anode compartments of the N-type electrolytic cell. The entire electrochemical test device was completely sealed with Vaseline and parafilm. Before electrochemical test, the electrolyte was purged with Ar (99.99%) gas for 30 min to remove oxygen. Linear sweep voltammetry (LSV) curves were recorded at a scan rate of 10 mV S^{-1} from -0.2 V to -0.7 V to ensure that the polarization curve is stable.

Quantification of ammonia

The concentration of NH_3, NO_3^- and NO_2^- was detected by the chromogenic methods via UV-vis technology in this work. Before UV-vis testing, the electrolytes were diluted to an appropriate concentration within the range of calibration curves. The chromogenic detection methods are as follow:

Detection of ammonia: The yield of NH_3 was detected via indophenol blue method. In brief, 1mL of electrolyte (after electrocatalysis) was extracted and diluted to an appropriate concentration in a sample bottle. 2 mL of NaOH solution (1 M) with 5 wt% sodium citrate and 5 wt% salicylic acid was then added to the 2 mL diluted electrolyte. After adding 1 mL of sodium hypochlorite (0.05 M) and 0.2mL of sodium nitroferricyanide (1 wt.%), the mixed solution was standing 2 h for coloration.

the UV-Vis absorption spectrum of these mixed solution was detected for analyzing the concentration of NH_3. Additionally, the absorbance calibration curve of NH_3 were obtained by testing ammonium chloride solutions with different concentrations.

The yield of NH_3 was calculated following the equation:

$$\text{Yield } NH_3 = (C_{NH_3} \times V)/(t \times A) \tag{2}$$

where C_{NH_3} means the NH_3 concentration, V: the volume of electrolyte, t: the electrocatalysis time, and A: the area of working electrode.

The faradaic efficiency (EF_{NH_3}) was calculated as follows:

$$FE_{NH_3} = (3F \times C_{NH_3} \times V)/(17 \times Q) \tag{3}$$

where F was the Faraday constant (96 485 C mol^{-1}), C_{NH_3}: the NH_3 concentration, and Q: the total charge in the electrocatalytic process

Detection of nitrate: In this work, 200 μL of electrolyte (after electrocatalysis) was extracted and diluted to an appropriate concentration in a sample bottle. 100 μL of HCl solution (1 M) and 10μL H_2SO_4 (0.08 M) were then added into the 5 mL diluted electrolyte. After standing 15 minutes, the UV-Vis absorption spectrum of these mixed solution was detected for analyzing the concentration of NO_3^-. The final absorbance of NO_3^- was confirmed by the following equation:

$$A = A_{220}-2A_{275} \tag{4}$$

Where A means the strength of the NO_3^- absorbance in UV-Vis spectrum, A_{220}: the absorption strength at the wavelength of 220 nm, A_{275}: the absorption strength at the wavelength of 270 nm.

The absorbance calibration curve of NO_3^- were obtained by testing sodium nitrate solutions with different concentrations.

Determination of nitrite: 1 mL of electrolyte (after electrocatalysis) was extracted and diluted to an appropriate concentration in a sample bottle. 100 mg of N-(1-naphthyl) ethylenediamine dihydrochloride, 2g of aminobenzenesulfonamide, and 5 mL of phosphoric acid were added into 25 mL of deionized water and mixed thoroughly as the color reagent. 0.1 mL of color reagent was added into 5 mL of diluted electrolyte. After standing 20 min, the UV-Vis absorption spectrum of these mixed solution was detected for analyzing the concentration of NO_2^-. The absorbance calibration curve of NO_2^- were obtained by testing sodium nitrite solutions with different concentrations.

Note: the chromogenic agent for nitrite is very unstable, which should be used as new configuration.

TOF calculation:

The TOF values were estimated as the following formula:

$$TOF = \frac{\text{Number of total ammonia turnover } / \ cm^2}{\text{Number of active sites } / \ cm^2} \tag{5}$$

The number of total ammonia turnovers was calculated from the current density and the Faraday efficiency by the following equation:

$$\text{Number of } NH_3 = \left(J\frac{mA}{cm^2}\right)(FE_{NH_3})\left(\frac{1\,C\,s^{-1}}{1000\,mA}\right)\left(\frac{1\,mol\,e^-}{96485.3\,C}\right)\left(\frac{1\,mol\,NH_3}{8\,mol\,e^-}\right)\left(\frac{6.022*10^{23}\,NH_3\,molecules}{1\,mol\,NH_3}\right) \tag{6}$$

The number of active sites was regarded as the number of surface sites, and calculated by the following formula:

$$\text{umber of active sites} = \left(\frac{\text{Number of metal site / unit cell}}{\dfrac{\text{Volume}}{\text{unit cell}}} \right)^{\frac{2}{3}} \tag{7}$$

Finally, the plot of current density can be converted into a TOF plot according to the following formula:

$$TOF = \frac{(\text{Number of } NH_3) * |J|}{\text{Number of active sites} * A_{ECSA}} \tag{8}$$

^{15}N Isotope Labeling Experiments

In order to confirm the source of NH_3, $Na^{15}NO_3$ ($\geq$ 98 atom% ^{15}N) was employed as ^{15}N labeling N-source. 0.1 M Na_2SO_4, adjusted to pH=11 by 0.1 M KOH, was used as the electrolyte and 0.1 M $Na^{15}NO_3$ was as the ^{15}N Isotope Labeled reactant. After 4 h electroreduction, the electrolyte in cathode compartment was taken out and adjusted pH value to 2 by 4M H_2SO_4 solution (4M). Then, deuterium oxide (D_2O) was added into the weak acid electrolyte for the further ^1H NMR detection with 600MHz.

DFT calculations

To investigate the electroreduction mechanism of nitrate, the single-layered Mo-HATN-MCOFs, Ni-HATN-MCOFs and HATN-MCOFs slabs were established, respectively. DFT calculations of these slabs were computed by using a generalized gradient approximation (GGA) of exchange-correlation functional in the Perdew, Burke, and Ernzerhof (PBE). GGA+U functional was used with an additional Coulomb potential $U = 2$ eV (Mo) and 3.1 eV (Ni) applied on states of 3d-orbit. A plane-wave energy cut off of 500 eV was used together with norm-conserving pseudopotentials, and the Brillouin zone was sampled with a $2 \times 2 \times 1$ Monkhorst–Pack grid. The structure was fully optimized until the force on each atom is less than 10^{-3} eV/Å. To avoid periodic interaction, a vacuum layer of 30 Å was incorporated into the slabs. The free energy (ΔG) was computed from

G E ZPE T S n e U = +

− Δ + Δ

$$\Delta G = \Delta E + ZPE - T\Delta S \tag{9}$$

where ΔE was the total energy, ZPE was the zero-point energy, the entropy (ΔS) of each adsorbed state were yielded from DFT calculation, whereas the thermodynamic corrections for gas molecules were from standard tables.

Results and Discussion

Figure S1. The chemical structure of HATN.

Figure S2. The chemical structure of (a) 1,2,4,5-tetraaminobenzene tetrahydrochloride and (b) hexaketocyclohexane
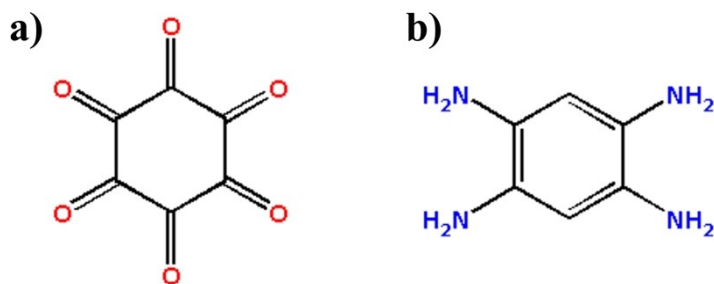

Figure S3. The XRD patterns of Mo-HATN-COFs, Ni-HATN-COFs and HATN-COFs samples.
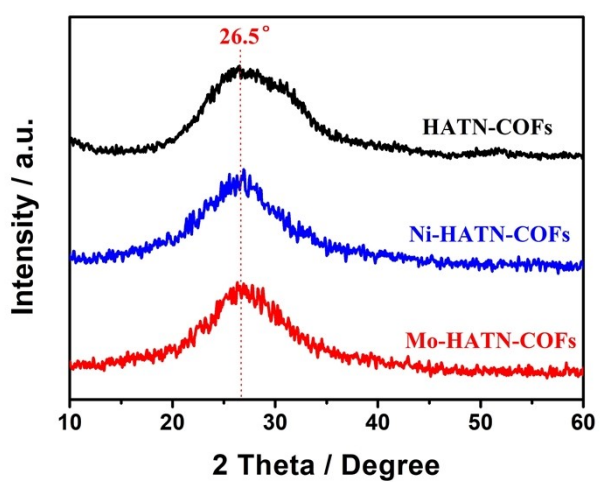
Figure S4. (a) The structure model of Mo-HATN-COFs. (b) The PDOS of Mo atoms in Mo-HATN-COFs.
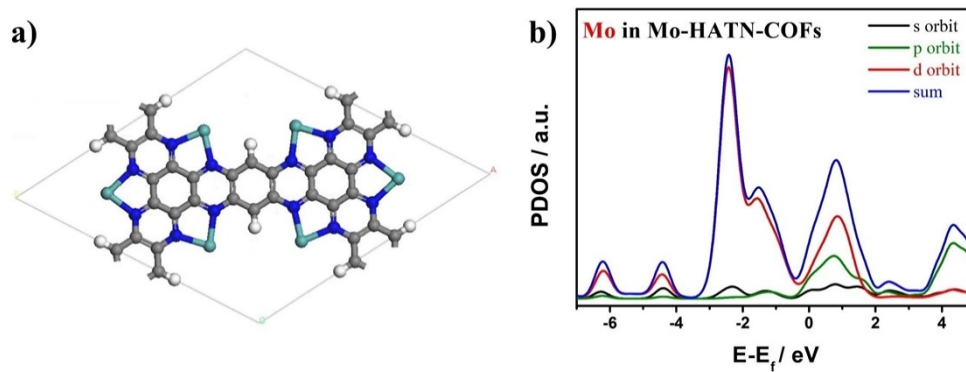

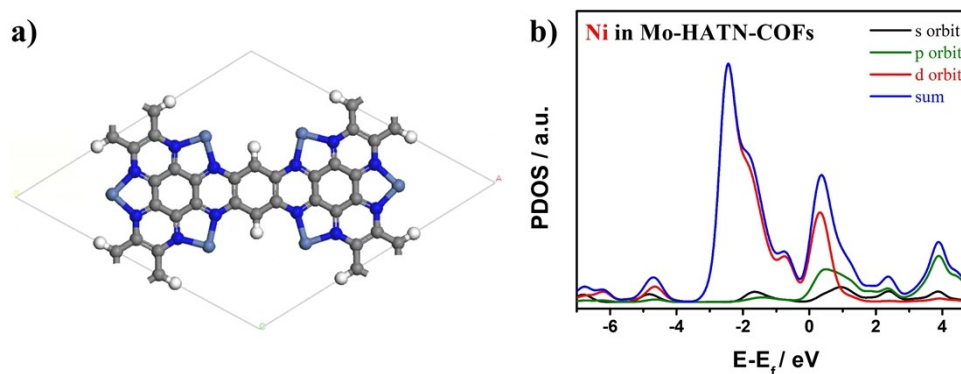Figure S5. (a) The structure model of Ni-HATN-COFs. (b) The PDOS of Ni atoms in Ni-HATN-COFs.

Figure S6. The d-orbit of Mo-HATN-COFs and Ni-HATN-COFs.
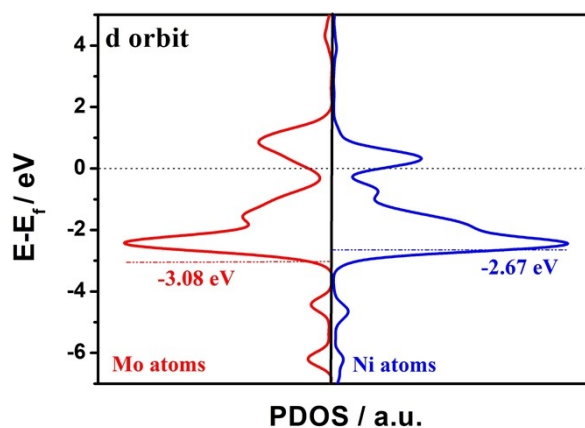
Figure S7. Nyquist plots of Mo-HATN-COFs and HATN-COFs.
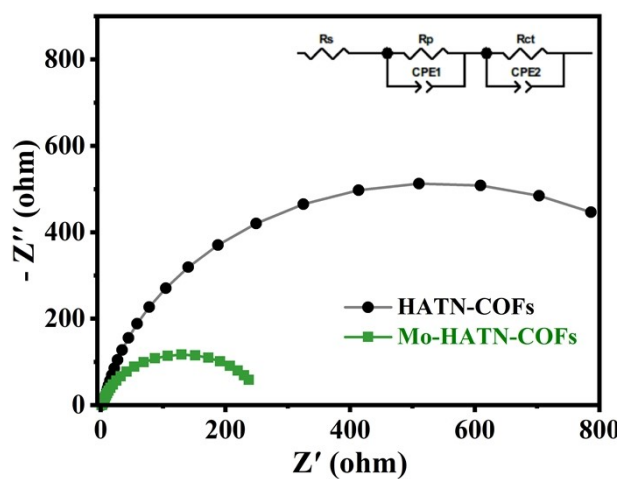
Figure S8. (a) The XRD pattern and (b) SEM image of NaCl template.
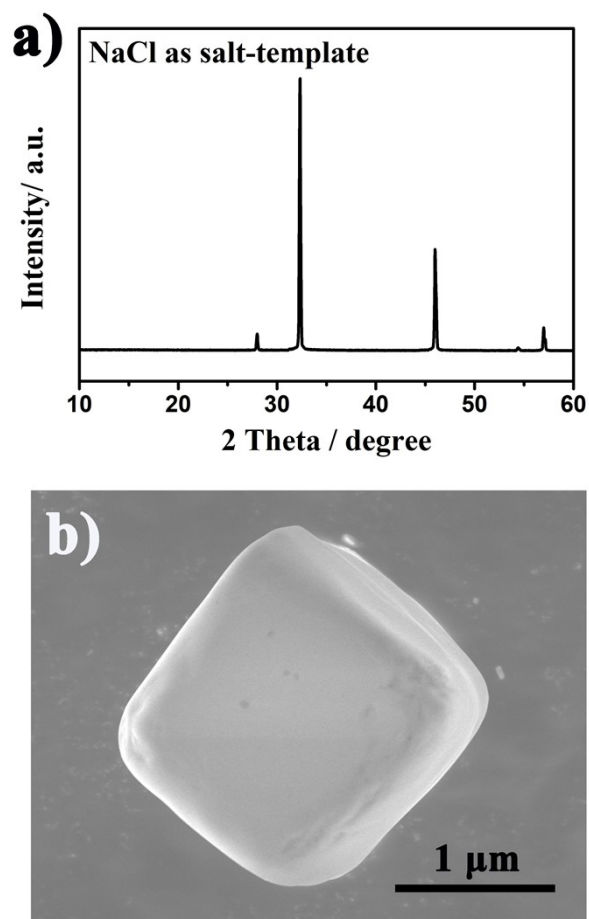
Figure S9. The high-solution SEM image of Mo-HATN-COFs.
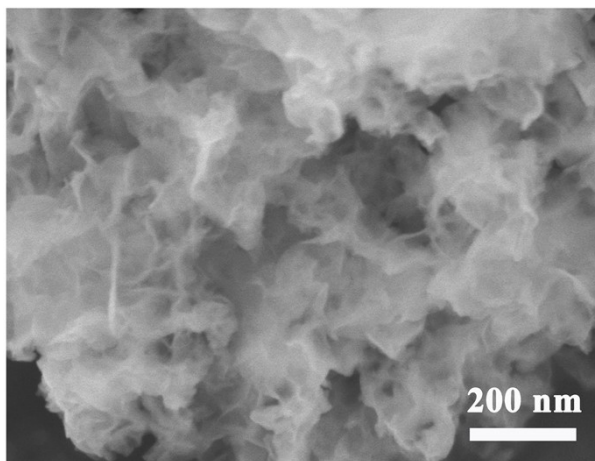
Figure S10. (a) The N$_2$ adsorption-desorption isotherm and (b) pore size distribution curve of Mo-HATN-COFs nanosheets
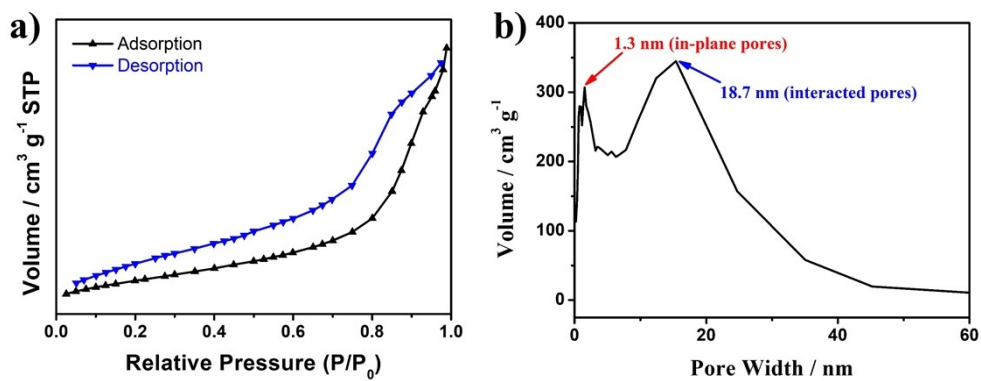
Figure S11. The SEM image of HATN-COFs nanosheets.
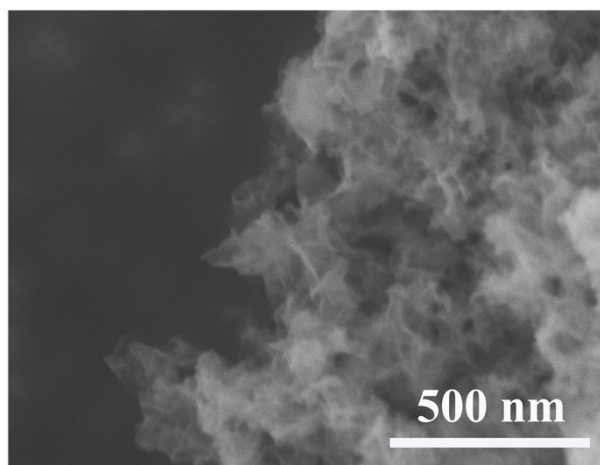
Figure S12. The high-solution TEM image of Ni-HATN-COFs nanosheets.
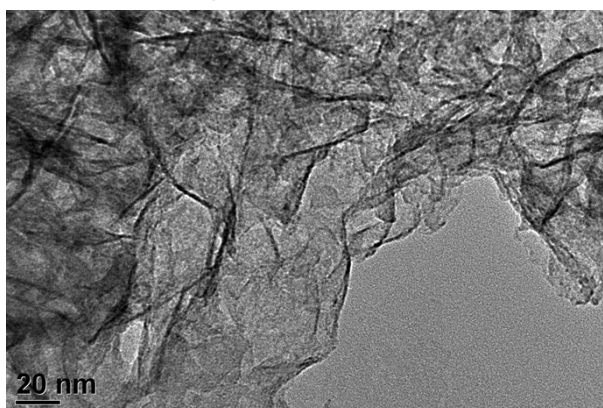
Figure S13. The high-solution TEM image of HATN-COFs nanosheets.
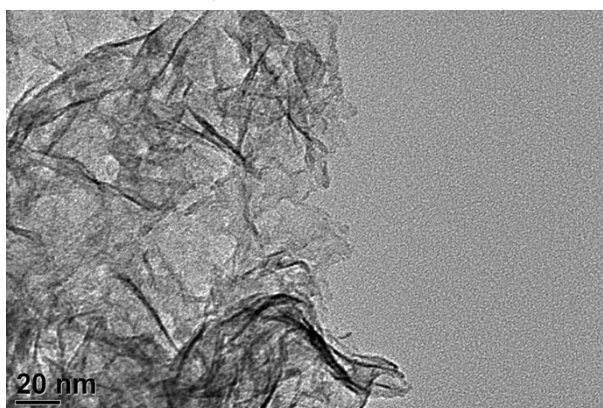
Figure S14. XPS spectra of (a) Mo 3d, (b) N 1s and (c) C1s in Mo-HATN-COFs.
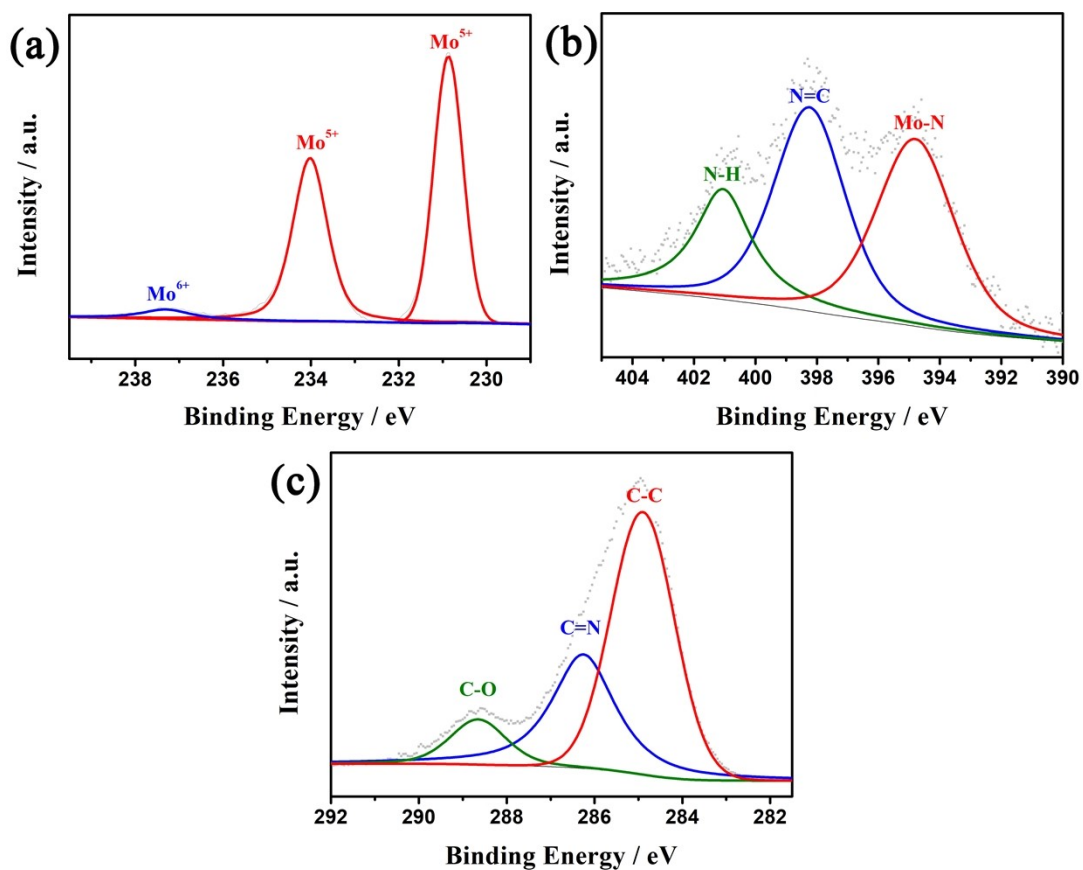
Figure S15. The diagram of the electrocatalytic reactor for nitrate reduction.
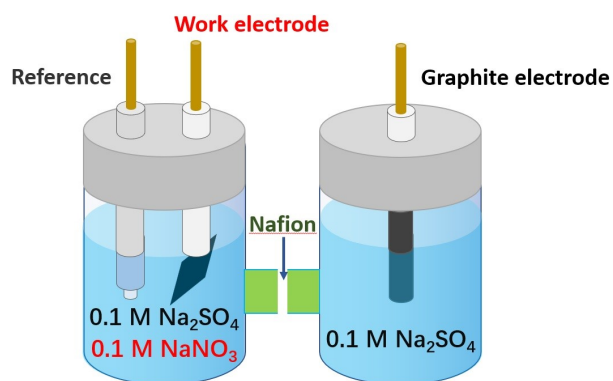
Figure S16. The SEM image of the surface of Mo-HATN-COFs electrode.
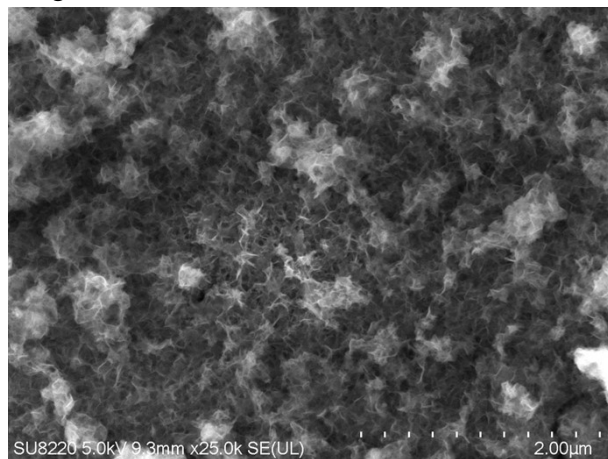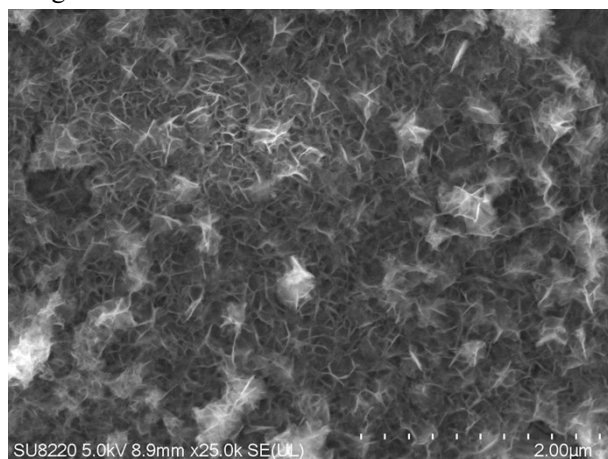

Figure S17. The SEM image of the surface of Ni-HATN-COFs electrode.

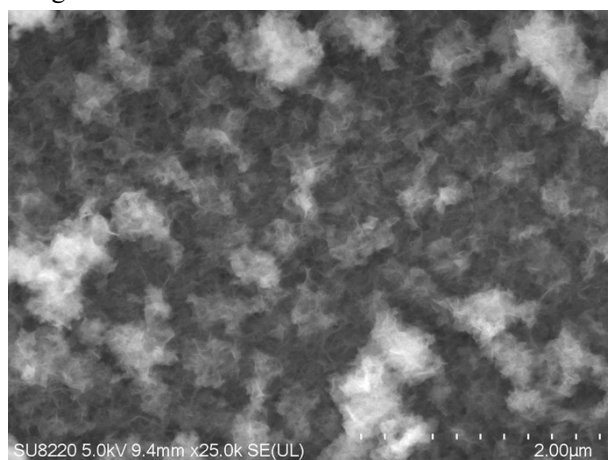Figure S18. The SEM image of the surface of HATN-COFs electrode.

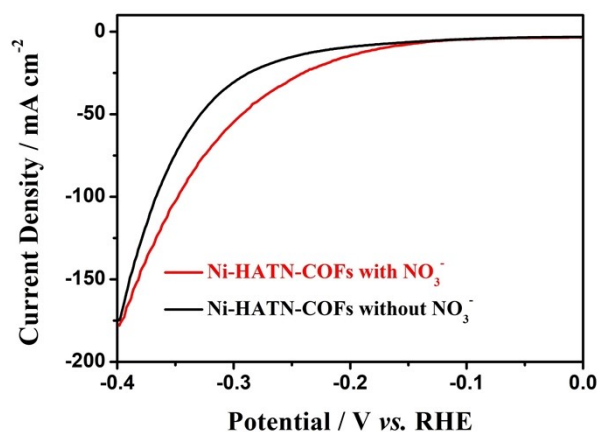Figure S19. The LSV curves of Ni-HATN-COFs with and without 0.1 M NaNO$_3$.

Figure S20. (a) The UV-vis absorption spectra with various NH$_4^+$ concentration in 0.5 M Na$_2$SO$_4$. b) The calibration curve used for estimation of the NH$_4^+$ concentration.
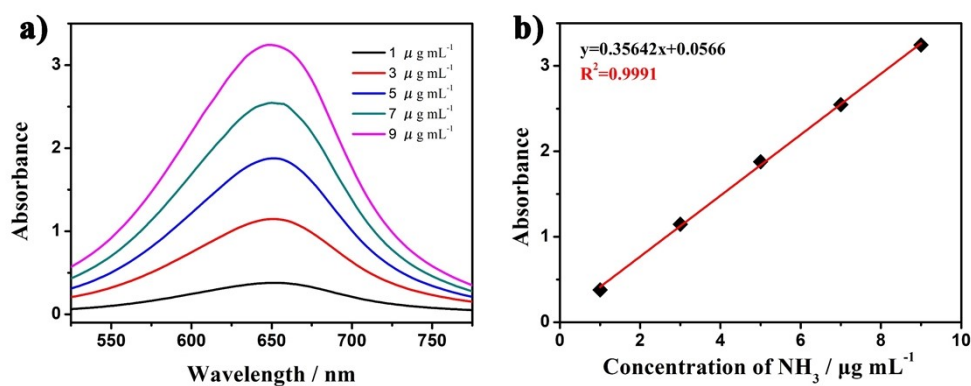

Figure S21. (a) The UV-vis absorption spectra with various NO$_2^-$ concentration. b) The calibration curve used for estimation of the NO$_2^-$ concentration.
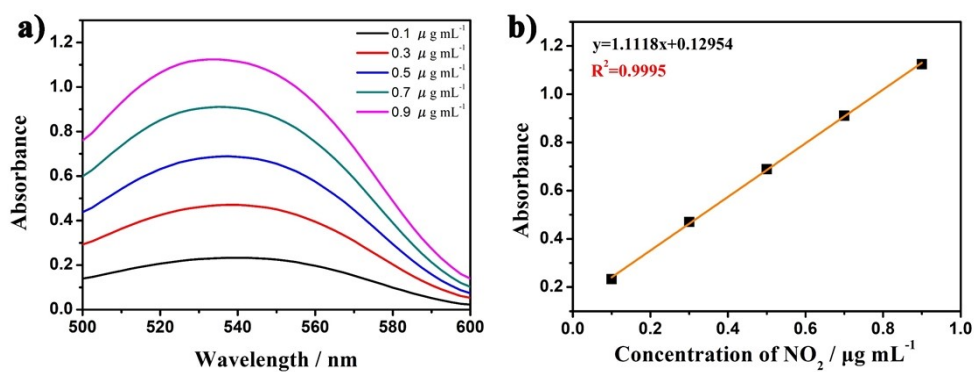
Figure S22. Potential-dependent yield rate and FE of ammonia over bulk Mo-HATN-COFs.
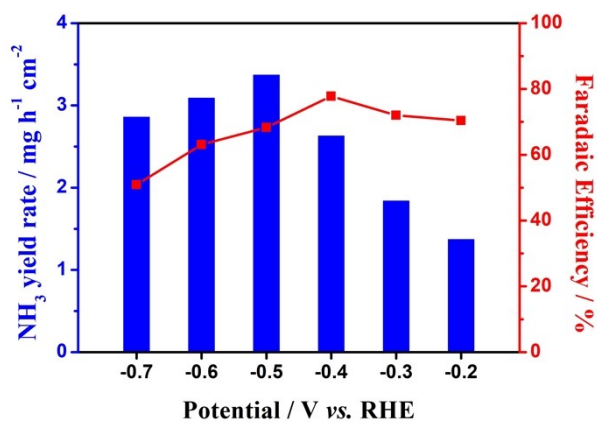

Figure S23. Potential-dependent yield rate and FE of ammonia over Ni-HATN-COFs nanosheets.
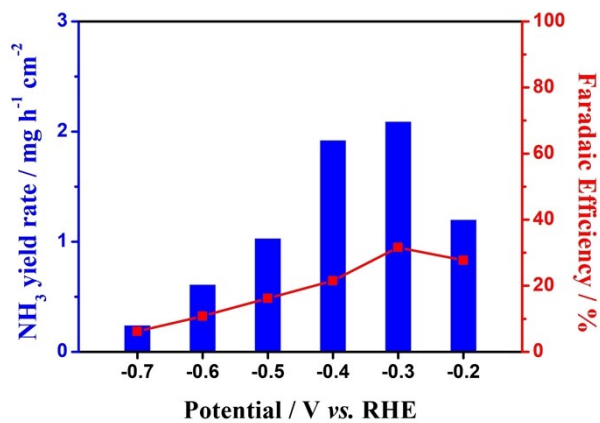

Figure S24. Potential-dependent yield rate and FE of ammonia over HATN-COFs nanosheets.
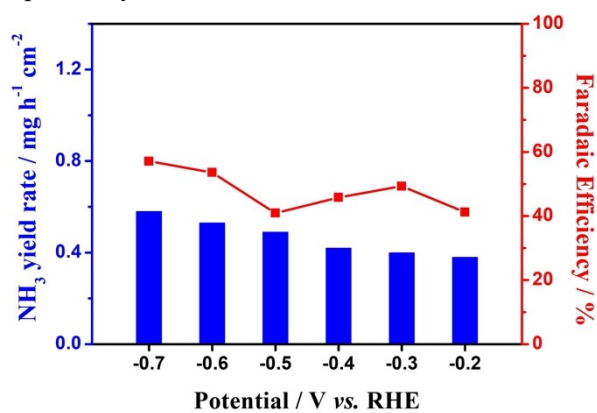
Figure S25. The ammonia yield rate of electrocatalysis over Mo-HATN-COFs within/without 0.1 M $NaNO_3$ electrolyte, and without applied potential in the presence of $NaNO_3$.
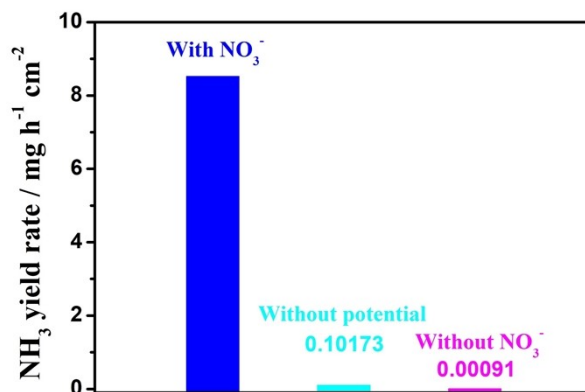

Figure S26. The XRD pattern of Mo-HATN-COFs after 10 h electrochemical reduction.
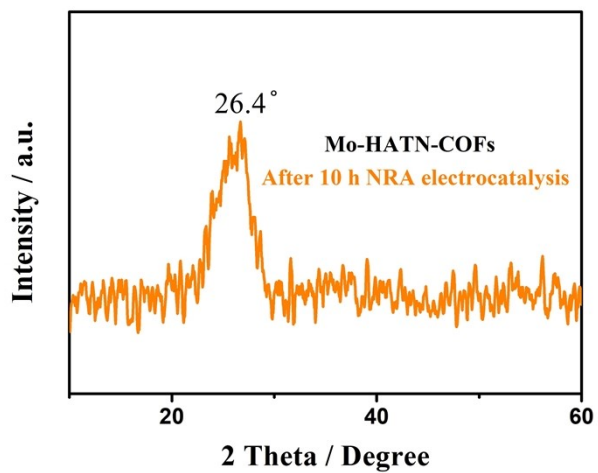
Figure S27. Structural models of single-layered Mo-HATN-COFs during NRA process (Mo cyan green atoms, N blue atoms, O red atoms and H white atoms).
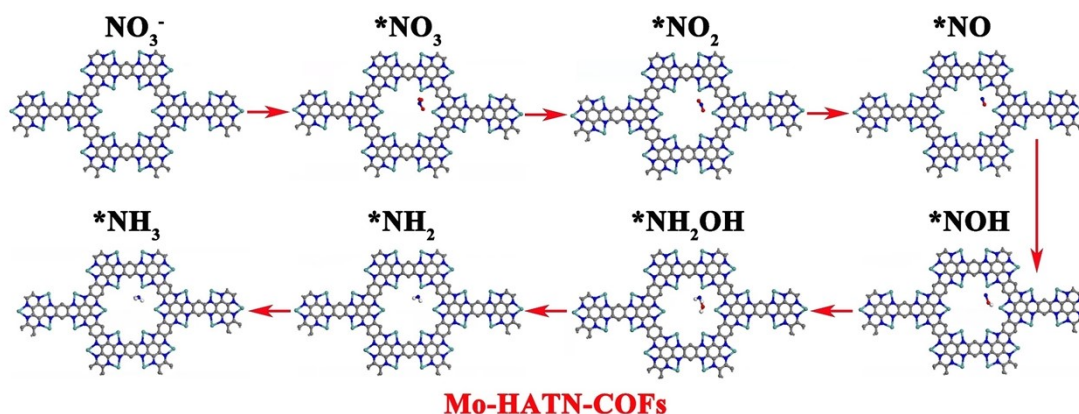

Figure S28. Structural models of single-layered Ni-HATN-COFs during NRA process (Ni light blue atoms, N blue atoms, O red atoms and H white atoms).
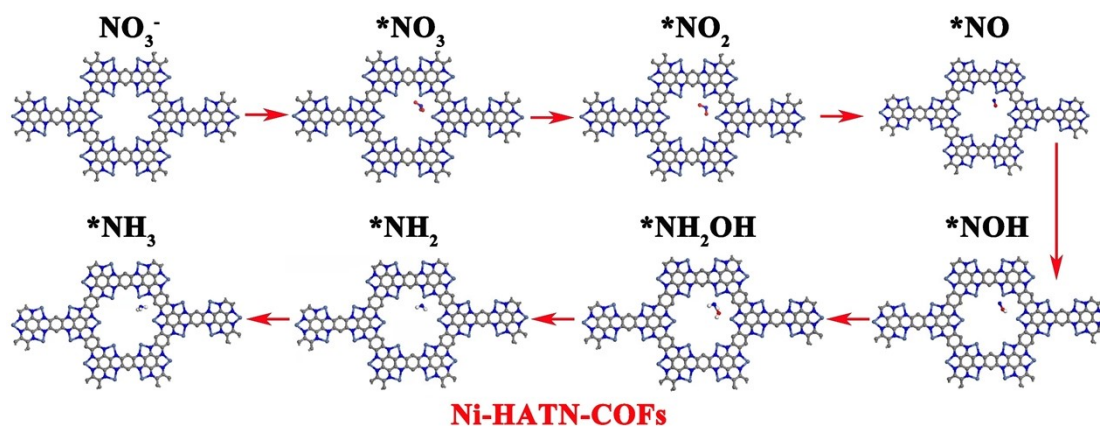

Figure S29. Structural models of single-layered HATN-COFs during NRA process (N blue atoms, O red atoms and H white atoms).
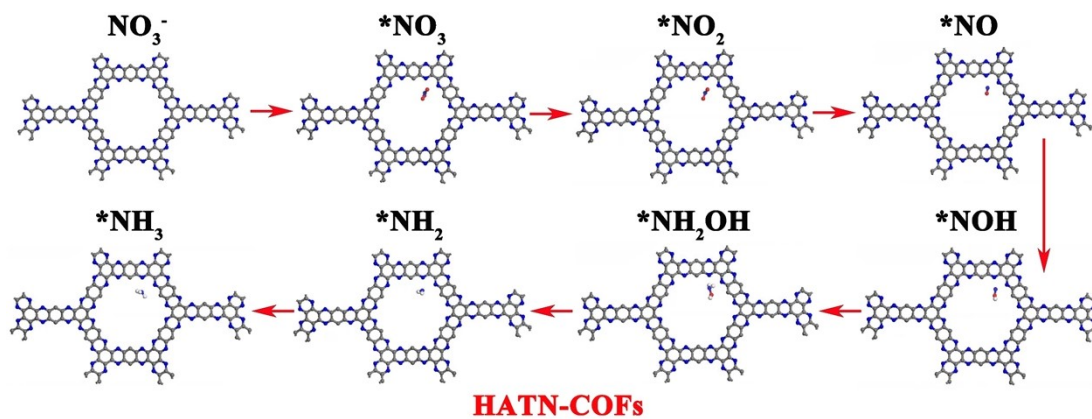
Figure S30. The charge density difference image of single-layered HATN-COFs with NO model
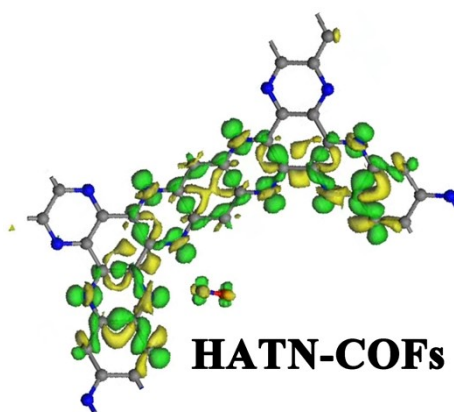

HATN-COFs

Table S1. The crystal structure of Mo-HATN-COFs, Ni-HATN-COFs and HATN-COFs

Sample	Symmetry	a=b (Å)	c(Å)	α=β (°)	γ (°)
Mo-HATN-COFs	P6/mmm	16.54	3.47	90	120
Ni-HATN-COFs	P6/mmm	16.48	3.48	90	120
HATN-COFs	P6/mmm	16.68	3.47	90	120

Table. S2 Comparison of electrocatalytic NRA performance of Mo-HATN-COFs with other MCOFs, Ni-MOFs electrocatalysts.

Sample	Electrolyte	Yield of NH$_3$	FE (%)	Reference
NiPr-TPA-COF	0.5 M Na$_2$SO$_4$ + 0.1 M NaNO$_3$	2.5 mg h^{-1} cm^{-2}	~90	[1]
Ce MOF-Cu	0.5 M Na$_2$SO$_4$ + 5 mM NaNO$_3$	66 μmol h^{-1} cm^{-2}	85.5	[2]
Cu@CuHHTP	0.5 M Na$_2$SO$_4$ + 500 ppm NO$_3^-$	1.84 mg h^{-1} cm^{-2}	67.55	[3]
RuNi-MOF	0.1 M Na$_2$SO$_4$ + 50 ppm NO$_3^-$	274 μg h^{-1} mg$^{-1}_{cat.}$	73	[4]
Ni-MOF	0.1 M Na$_2$SO$_4$ + 1.5 g/L NaNO$_3$.	110.13 ug h^{-1} cm^{-2}	12.6	[5]
Fe$_2$Co-MOF	0.05 M H$_2$SO$_4$ + 50 g/L KNO$_3$	2686.33 μg h^{-1} mg$^{-1}_{cat.}$	90.55	[6]
Zr-MOF	0.1 M Na$_2$SO$_4$ + 500 ppm NO$_3^-$	287.31 μmol h^{-1} cm^{-2}	58.1	[7]
UiO-CuZn	0.5 M Na$_2$SO$_4$ + 200 ppm NO$_3^-$	0.228 mmol h^{-1} g^{-2}	91.4	[8]
NiPc-CNT	361.1mg/L KNO$_3$	—	86.8	[9]
CuNi/NC	0.1 M PBS + 50ppm	—	79.6	[10]
Mo-HATN-COFs	0.1 M Na$_2$SO$_4$ + 0.1 M NaNO$_3$	8.52 mg h^{-1} cm^{-2}	91.3	This work

References:

[1] F. Lv, M. Sun, Y. Hu, J. Xu, W. Huang, N. Han, B. Huang, Y. Li, *Energy Environ. Sci.*, **2023**, *16*, 201.

[2] Y.-T. Xu, M.-Y. Xie, H. Zhong and Y. Cao, *ACS Catal.*, **2022**, *12*, 8698-8706.

[3] X. Zhu, H. Huang, H. Zhang, Y. Zhang, P. Shi, K. Qu, S.-B. Cheng, A.-L. Wang, Q. Lu, *ACS Appl. Mater. Interfaces*, **2022**, *14*, 32176-32182.

[4] J. Qin, K. Wu, L. Chen, X. Wang, Q. Zhao, B. Liu and Z. Ye, *J. Mater. Chem. A*, **2022**, *10*, 3963-3969.

[5] F. Pan, J. Zhou, T. Wang, Y. Zhu, H. Ma, J. Niu, C. Wang, *J. Colloid. Interf. Sci.*, **2023**, *638*, 26-38.

[6] Y. Lv, S.-W. Ke, Y. Gu, B. Tian, L. Tang, P. Ran, Y. Zhao, J. Ma, J.-L. Zuo, M. Ding, *Angew. Chem. Int. Ed.*, **2023**, *62*, e202305246.

[7] M. Jiang, J. Su, X. Song, P. Zhang, M. Zhu, L. Qin, Z. Tie, J.-L. Zuo, Z. Jin, *Nano Lett.*, **2022**, *22*, 2529-2537.

[8] Z. Wang, S. Liu, M. Wang, L. Zhang, Y. Jiang, T. Qian, J. Xiong, C. Yang, C. Yan, *ACS Catal.*, **2023**, *13*, 9125-9135.

[9] Y. Li, L. Ren, Z. Li, T. Wang, Z. Wu, Z. Wang, *ACS Appl. Mater. Interfaces*, **2022**, *14*, 53884-53892.

[10] Y. Liu, B. Deng, K. Li, H. Wang, Y. Sun, F. Dong, *J. Colloid Interface Sci.*, **2022**, *614*, 405-414.